Single Dirac Cone Topological Surface State and Unusual Thermoelectric Property of Compounds from a New Topological Insulator Family

Y. L. Chen,[1,2,3] Z. K. Liu,[1,2] J. G. Analytis,[1,2] J.-H. Chu,[1,2] H. J. Zhang,[1,2] B. H. Yan,[1,2] S.-K. Mo,[3] R. G. Moore,[1] D. H. Lu,[1] I. R. Fisher,[1,2] S. C. Zhang,[1,2] Z. Hussain,[3] and Z.-X. Shen[1,2]

[1]*Stanford Institute for Materials and Energy Sciences, SLAC National Accelerator Laboratory, 2575 Sand Hill Road, Menlo Park, California 94025, USA*

[2]*Geballe Laboratory for Advanced Materials, Departments of Physics and Applied Physics, Stanford University, Stanford, California 94305, USA*

[3]*Advanced Light Source, Lawrence Berkeley National Laboratory, Berkeley, California 94720, USA*

(Received 26 July 2010; revised manuscript received 19 October 2010; published 20 December 2010)

Angle resolved photoemission spectroscopy study on $TlBiTe_2$ and $TlBiSe_2$ from a thallium-based ternary chalcogenides family revealed a single surface Dirac cone at the center of the Brillouin zone for both compounds. For $TlBiSe_2$, the large bulk gap (~ 200 meV) makes it a topological insulator with better mechanical properties than the previous binary 3D topological insualtor family. For $TlBiTe_2$, the observed negative bulk gap indicates it as a semimetal, instead of a narrow-gap semiconductor as conventionally believed; this semimetality naturally explains its mysteriously small thermoelectric figure of merit comparing to other compounds in the family. Finally, the unique band structures of $TlBiTe_2$ also suggest it as a candidate for topological superconductors.

DOI: 10.1103/PhysRevLett.105.266401 PACS numbers: 71.18.+y, 71.20.−b, 73.20.−r, 73.23.−b

Topological insulators represent a new state of quantum matter with a bulk gap and odd number of relativistic Dirac fermions on the surface [1]. Since the discovery of the two dimensional (2D) topological insulator in HgTe quantum well [2,3] and the subsequent discovery in 3D materials (especially the single Dirac cone family Bi_2Te_3, Bi_2Se_3 and Sb_2Te_3) [4–6], topological insulators has grown as one of the most intensively studied fields in condensed matter physics [1–14]. Moreover, the massless Dirac fermions and the magnetism in topological insulators can further link them to relativity and high energy physics [15]. The fast development of topological insulators also inspires the study of other topological states such as topological superconductors [11–13,16,17], which have a pairing gap in the bulk and a topologically protected surface state consisting of Majorana fermions [11]. Unlike Dirac fermions in topological insulators that can have the form of particles or holes, Majorana fermions are their own antiparticles [18]. The simplest 3D topological superconductor consists of a single Majorana cone on the surface, containing half the degree of freedom of the Dirac surface state of a single cone 3D topological insulator. This fractionalization of the degree of freedom introduces quantum nonlocality and is essential to the topological quantum computing based on Majorana fermions [19].

In this work, we use ARPES to study $TlBiTe_2$ and $TlBiSe_2$ from a recently proposed topological insulator family of thallium-based ternary chalcogenides [14,20]. Remarkably, a single Dirac cone centered at the point of the surface Brillouin zone (BZ) is found in both materials, and the surface and bulk electronic structures measured by ARPES are in broad agreement with *ab initio* calculations. Furthermore, for the *p*-type $TlBiTe_2$, the experimental band structure reveals six leaflike bulk pockets around the surface Dirac cone. Given that these bulk pockets are the only structure other than the Dirac cone on the Fermi surface (FS), they provide a possible origin for the reported bulk superconductivity[21], which can further induce superconductivity to the surface state by proximity effect, making $TlBiTe_2$ a possible candidate for 3D topological superconductors. Another compound of the family, $TlBiSe_2$ has a simpler bulk structure around the Dirac cone at Γ while the Dirac point resides in the bulk energy gap (~ 200 meV), making it a large gap topological insulator similar to Bi_2Se_3 [4], but with much better mechanical properties, as the covalence bonding between atomic layers in $TlBiSe_2$ is much stronger [14] than the van de Waals' force that bonds quintuple layer units of Bi_2Te_3 or Bi_2Se_3 [4].

Interestingly, the ternary III-V-VI_2 family compounds are also known as good high-temperature themoelectric materials [22–27], and a long-standing puzzle since the 1960s has been the unusually low themoelectric figure of merit (ZT) of $TlBiTe_2$ ($ZT \sim 0.15$) due to its much smaller thermoelectric power S ($\sim 70\ \mu V/K$) [22,24] comparing to that of other compounds ($ZT \sim 0.9$, $S \sim 200\ \mu V/K$) [25,26] in the family. By observing a negative band gap in the band structure, we demonstrate that $TlBiTe_2$ is a semimetal, in contrast to a narrow-gap semiconductor as conventionally believed [23,27], thus naturally explaining its mysteriously small thermoelectric power, as will be discussed later in the Letter.

The crystal structure of $TlBiTe_2$ is shown in Fig. 1. The x-ray diffraction, Laue and low energy electron diffraction

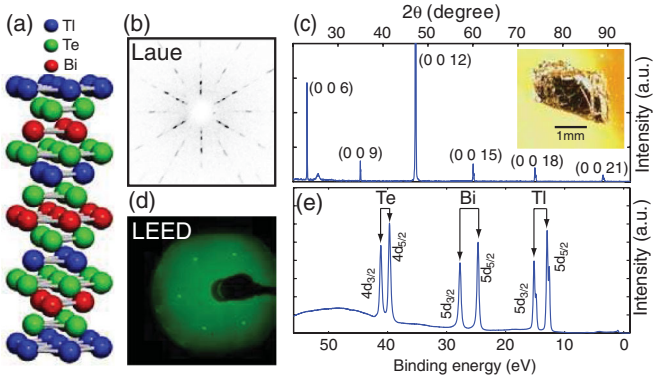

FIG. 1 (color). (a) Crystal structure of $TlBiTe_2$ with repeating Tl-Te-Bi-Te layers. (b),(c) Laue and x-ray diffraction characterizations show the high quality of the crystal. Inset in (c) shows a flat cleavage surface along (111) direction. (d) LEED pattern acquired after ARPES demonstrates clear diffraction spots without surface reconstruction. (e) Core level photoemission spectrum shows the d-shell electron peaks of all three compositional elements.

(LEED) characterizations all show the high quality of the samples used in this work.

The band structure of $TlBiTe_2$ at the BZ center is presented in Fig. 2, where the 3D plot [Fig. 2(a)] shows a clear Dirac cone centered at Γ surrounded by broad features from the bulk conduction (BCB) and valence band (BVB). To confirm the surface nature of the Dirac cone, photon energy dependent ARPES study (Fig. 2(b) [28]) was performed. The nonvarying shape of the outer hexagonal surface state band (SSB) FS under different photon energies indicates its 2D nature, while the shape and the existence of the BCB FS pocket inside changes dramatically due to its 3D nature with strong k_z dispersion.

Detailed band dispersions along Γ-M and Γ-K directions are illustrated in Fig. 2(c). The linear dispersion of the SSB clearly indicate a massless Dirac fermion with a velocity of $\sim 6.23 \times 10^5$ m/s (4.11 eV $\cdot$ Å [28]), about 1.5 times larger than the value in Bi_2Te_3 [6]. The broad features come from the bulk bands, among which an asymmetry of the BVB between the two directions can be seen. Based on the characteristic energy positions of the bulk band, we can divide the band structure into four regions [Fig. 2(c)] for the discussion of different FS geometries [Fig. 2(d)]. From region I to III, the bulk contribution evolves from an n-type pocket inside (region I) the n-type SSB FS to six p-type leaflike pockets outside (region III), with the bulk pockets disappearing in region II, while in region IV, both the SSB pocket at the center and the surrounding leaflike bulk pockets are p type.

Besides having the single surface Dirac cone, $TlBiTe_2$ was also reported to superconduct when p doped (with the hole density $\sim 6 \times 10^{20}/\mathrm{cm}^3$) [21]. At this doping, the E_F of the system is ~ 150 meV below the BCB bottom and resides in region III, where the FS geometry is characterized by a ringlike SSB FS and six surrounding p-type bulk pockets [Fig. 3(a)], as clearly shown in the region III plot of Fig. 2(d). A broad scan in k space covering four BZs [Fig. 3(b)] confirms that the FS structure shown in Fig. 3(a) is the only feature within each BZ. This naturally indicates that the bulk superconductivity of p-type $TlBiTe_2$ originates from the six leaflike bulk pockets, and in the superconducting state, the surface state [the center FS pocket in Figs. 3(a) and 3(b)] can become superconducting due to the proximity effect induced by the bulk superconductivity. For such a superconductor, it has been proposed [11] that each vortex line has two Majorana zero modes related by the time reversal symmetry, making it a candidate for the long sought after topological superconductors and suitable for the topological quantum computation [19]. However, the presence of superconductivity in p-type $TlBiTe_2$ requires further confirmation [29].

The band structures of $TlBiTe_2$ in larger energy and momentum range are shown in Fig. 3(c) [28]. In general,

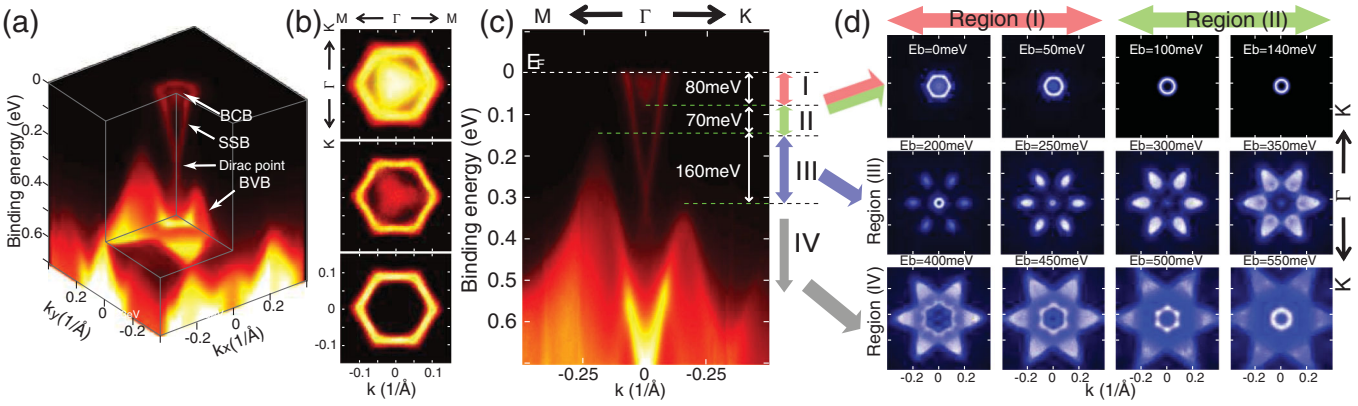

FIG. 2 (color). (a) 3D band structure of $TlBiTe_2$, with the BCB, BVB, SSB, and the Dirac point indicated. (b) FS maps (symmetrized according to the crystal symmetry) for 21, 23, and 25 eV photons. (c) Dispersion along M-Γ-K direction. Four regions defined by characteristic energy positions are labeled as I, II, III, and IV. (d) Constant energy plots of the band structure from different regions defined in (c), showing the BCB FS inside SSB (region I), SSB only (region II), BVB outside SSB (region III) and all BVB (region IV).

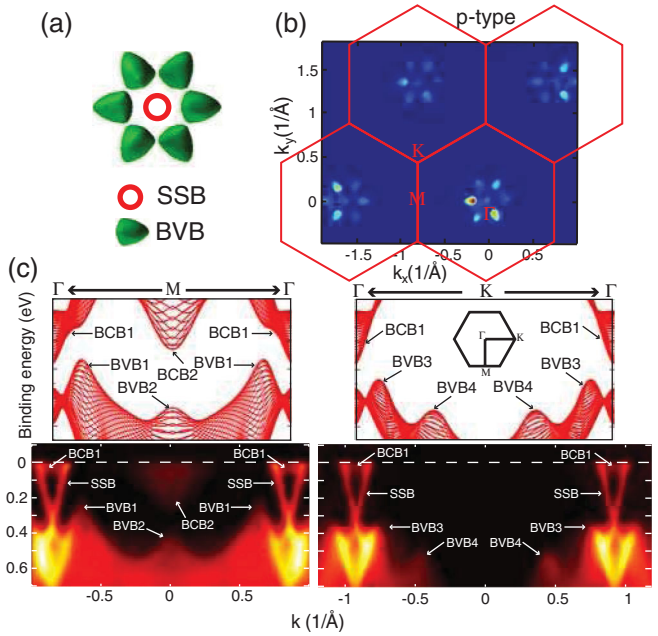

FIG. 3 (color). (a) Typical FS geometry in region III as defined in Fig. 2. (b) Broad k-space scan shows no additional features besides the FS pockets illustrated in (a). High symmetry points Γ, M, and K are marked; the uneven intensity at different BZs results from the matrix element effect. (c) Comparison between the *ab initio* calculation (top panels) and experimental band structures (bottom panels), with the prominent BCB, BVB, and SSB features labeled.

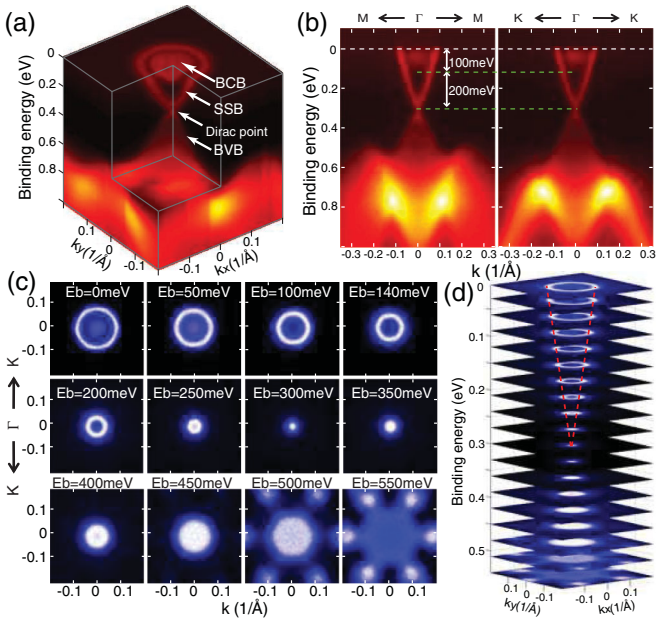

FIG. 4 (color). (a) 3D illustration of the band structure of $TlBiSe_2$ around Γ, with the BCB, BVB, SSB, and the Dirac point indicated. (b) Detailed band structure along M-Γ-M and K-Γ-K directions, with less anisotropy compared to Fig. 2(c). The bottom of the BCB at Γ is ~100 meV below E_F and the Dirac point residing on top of the BVB is ~200 meV below the BCB bottom. The smearing of the distinct SSB below the Dirac point is due to the hybridization with the BVB. (c) Constant energy contours of the band structure at different binding energies. (d) Stacking constant energy plots shows the evolution of the band structure. Red dashed line traces the dispersion of the SSB from the Dirac point.

the experimental dispersions along both directions agree well with the calculation, which reproduces each bulk feature of the measurement [Fig. 3(c)] except for an important difference, that the ARPES measurement [Fig. 3(c), bottom left panel] clearly shows a negative energy gap (~ 20 meV) between the electron pocket (BCB2) bottom at M and the valence band (BVB1) top near Γ (BVB1). This negative band gap shows that the $TlBiTe_2$ is a semimetal if E_F resides inside this region.

This semimetalicity of $TlBiTe_2$ not only corrects the conventional misunderstanding that it is a narrow-gap semiconductor [23,27], but also naturally solves the mysterious puzzle of the small thermoelectric power of $TlBiTe_2$ [22,24]. Since electrons and holes have opposite signs for their thermoelectric power S, the coexistence of the conduction electron (near Γ) and hole (at M) pockets (due to the negative band gap between BCB2 and BVB1) results in a greatly reduced S because of the cancellation of their opposite contributions. As the thermoelectric figure of merit $ZT = S^2\sigma/\kappa T$ (where σ and κ are the electric and thermal conductivity, respectively), the greatly reduced S leads to even further suppressed ZT due to its quadratic dependence on S.

The band structure of $TlBiSe_2$, another compound from the Tl-based ternary family, is summarized in Fig. 4 (band structure near Γ) and Fig. 5 (broad k-space scans) [28]. Similar to $TlBiTe_2$, the existence of a single surface Dirac cone at the Γ point (with a velocity of $\sim 6.85 \times 10^5$ m/s ,or 4.52 eV · Å [28], slightly larger than that of $TlBiTe_2$) can be seen in both figures, confirming its topological nontriviality.

The main difference between $TlBiSe_2$ and $TlBiTe_2$ is that the Dirac point of $TlBiSe_2$ resides on the BVB top [Figs. 4(a) and 4(b)], and the bulk gap at Γ (~ 200 meV, see Fig. 4(b) [28])is much larger than the energy scale of room temperature (26 meV), making it a large gap topological insulator suitable for promising applications in low-power electronic and spintronic devices at room temperature. Compared to the previously found 3D topological insulator family Bi_2Te_3/Bi_2Se_3 where the quintuple layer units are bonded by van de Waal's force [4], the much improved mechanical properties of $TlBiTe_2$ that resulted from the covalence boding between atomic layers [14] make it more favorable for real world devices.

In addition, the bulk band structure of $TlBiSe_2$ is simpler around Γ and less anisotropic between Γ-M and Γ-K directions [Figs. 4(a) and 4(b)] compared to that of $TlBiTe_2$ [Figs. 2(a) and 2(c)]. This simplicity can also be seen in the constant energy contour plots [Fig. 4(c)] and its

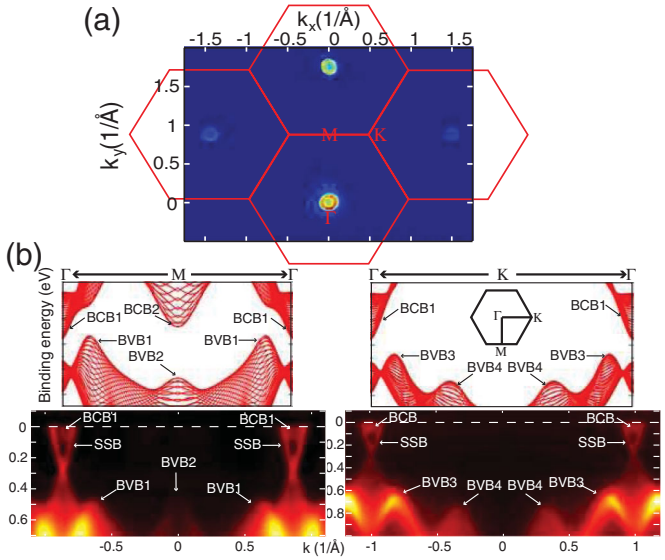

FIG. 5 (color). (a) Broad FS map of n-type $TlBiSe_2$ shows a FS sheet without BCB pocket at M point. (b) Comparison between the calculation (top panels) and measured band structure (bottom panels). Results along Γ-M-Γ and Γ-K-Γ directions are shown on the left and right rows, respectively. Prominent BCB, BVB, and SSB features are marked in both the calculated and measured band structures.

evolution [Fig. 4(d)]. Comparing Fig. 4(c) to Fig. 2(b), we notice that the SSB FS of $TlBiSe_2$ is a convex hexagon, in contrast to that of $TlBiTe_2$ which shows slightly concave geometry. This difference resembles the difference between the SSB FSs of Bi_2Te_3 and Bi_2Se_3, and can be reflected by different observations in experiments such as scanning tunneling microscopy or spectroscopy STM/STS [30,31].

Besides the simpler band geometry around Γ, broad range band structure (Fig. 5) of $TlBiSe_2$ is also less complicated without the electron pocket at M point, as shown in both the FS map [Fig. 5(a)] and the dispersion plots [Fig. 5(b), bottom row]. Also, although the comparison between the experiments and calculation [Fig. 5(b)] again shows broad agreement, the BCB2 feature at M point in the calculation (top left panel) was not seen in the measurements (bottom left panel), causing the missing of an electron pocket at M point in Fig. 5(a).

In summary, the identification of the single Dirac cone surface state in both $TlBiTe_2$/$TlBiSe_2$ and the possibility of the topological superconducting phase in $TlBiTe_2$ extends the study of topological quantum phases to a new family of materials, and the better physical properties of these ternary chalcogenides make the realization of applications more realistic. Furthermore, our finding of the semimetalicity in $TlBiTe_2$ solves the long-standing puzzle of the unique thermoelectric properties of $TlBiTe_2$ in this family of high-temperature thermoelectric materials.

We thank X. L. Qi and C. X. Liu for insightful discussions. This work is supported by the Department of Energy, Office of Basic Energy Science under Contract No. DE-AC02-76SF00515.

[1] X. L. Qi and S. C. Zhang, Phys. Today **63**, No. 1, 33 (2010).
[2] A. Bernevig, T. L. Hughes, and S. C. Zhang, Science **314**, 1757 (2006).
[3] M. Konig *et al.*, Science **318**, 766 (2007).
[4] H. Zhang *et al.*, Nature Phys. **5**, 438 (2009).
[5] Y. Xia *et al.*, Nature Phys. **5**, 398 (2009).
[6] Y. L. Chen *et al.*, Science **325**, 178 (2009).
[7] L. Fu, C. L. Kane, and E. J. Mele, Phys. Rev. Lett. **98**, 106803 (2007).
[8] X. L. Qi, T. L. Hughes, and S. C. Zhang, Phys. Rev. B **78**, 195424 (2008).
[9] J. E. Moore and L. Balents, Phys. Rev. B **75**, 121306(R) (2007).
[10] R. Roy, Phys. Rev. B **79**, 195321 (2009).
[11] X. L. Qi *et al.*, Phys. Rev. Lett. **102**, 187001 (2009).
[12] L. Fu and E. Berg, Phys. Rev. Lett. **105**, 097001 (2010).
[13] Y. S. Hor *et al.*, arXiv:1006.0317.
[14] B. Yan *et al.*, Europhys. Lett. **90**, 37002 (2010).
[15] F. Wilczek, Nature (London) **458**, 129 (2009).
[16] X. L. Qi, T. L. Hughes, and S. C. Zhang, Phys. Rev. B **81**, 134508 (2010).
[17] A. P. Schnyder *et al.*, Phys. Rev. B **78**, 195125 (2008).
[18] F. Wilczek, Nature Phys. **5**, 614 (2009).
[19] C. Nayak *et al.*, Rev. Mod. Phys. **80**, 1083 (2008).
[20] H. Lin *et al.*, Phys. Rev. Lett. **105**, 036404 (2010).
[21] R. Hein and E. Swiggard, Phys. Rev. Lett. **24**, 53 (1970).
[22] D. P. Spitzer and J. A. Kykes, J. Appl. Phys. **37**, 1563 (1966).
[23] K. Chrissafis *et al.*, Phys. Status Solidi A **196**, 515 (2003).
[24] K. Kurosaki, A. Kosuga, and S. Yamanaka, J. Alloys Compd. **351**, 279 (2003).
[25] K. Kurosaki *et al.*, J. Alloys Compd. **376**, 43 (2004).
[26] K. F. Hsu *et al.*, Science **303**, 818 (2004).
[27] K. Hoang and S. D. Mahanti, Phys. Rev. B **77**, 205107 (2008).
[28] See supplementary material at http://link.aps.org/supplemental/10.1103/PhysRevLett.105.266401.
[29] J. D. Jensen *et al.*, Phys. Rev. B **6**, 319 (1972).
[30] L. Fu, Phys. Rev. Lett. **103**, 266801 (2009).
[31] Z. Alpichshev *et al.*, Phys. Rev. Lett. **104**, 016401 (2010).